Journal of Applied Polymer Science

Influences of pre-ordered melt structures on the crystallization behavior and polymorphic composition of β-nucleated isotactic polypropylene with different stereo-defect distribution

Jian Kang,[1] Gengsheng Weng,[2] Jinyao Chen,[1] Feng Yang,[1] Ya Cao,[1] Ming Xiang[1]

[1]State Key Laboratory of Polymer Materials Engineering, Polymer Research Institute of Sichuan University, Chengdu 610065, People's Republic of China

[2]Faculty of Materials and Chemical Engineering, Ningbo University, Ningbo 315211, People's Republic of China

Corresponding to: F. Yang (E-mail: yangfengscu@126.com)

ABSTRACT: As part of continuous efforts to understand the surprising synergetic effect between β-nucleating agent and pre-ordered structures of isotactic polypropylene (iPP) in significant enhancement of β-crystallization (Ordered Structure Effect, OSE), two β-nucleated iPP with different uniformities of stereo-defect distribution (WPP-A and WPP-B) were prepared, their crystallization behaviors with variation of melt structures were studied in detail. The results revealed that β-phase can hardly form in WPP-A (whose stereo-defect distribution is less uniform) because of its strong tendency of α-nucleation caused by its less uniform stereo-defect distribution, while WPP-B is more favorable for β-crystallization; As fusion temperature decreases, similar variation trends of crystallization temperature and β-phase proportion can be observed from WPP-A and WPP-B, indicating the occurrence of OSE behavior, which provides unsurpassed β-nucleation efficiency and induces β-crystallization even in WPP-A which is less favorable for β-crystallization; moreover, the upper and lower limiting temperatures of Region II of WPP-A and WPP-B are identical, suggesting the uniformity of stereo-defect distribution has little influence on temperature window for OSE (denoted as Region II). To explore the physical nature of Region II, self-nucleation behavior and equilibrium melting temperature (T_m^0) of PP-A and PP-B were studied. The lower limiting temperatures of exclusive self-nucleation domain of both PP-A and PP-B are identical with the lower limiting temperatures of Region II in OSE (168°C); moreover, the $T_m{}^0$ of both PP-A and PP-B are close to their upper limiting temperatures of Region II in OSE behavior (189°C). The possible explanation was proposed. © 2015 Wiley Periodicals, Inc. J. Appl. Polym. Sci. **2015**, *132*, 42632.

KEYWORDS: crystallization; polyolefins; structure–property relations; thermal properties

Received 14 March 2015; accepted 19 June 2015

DOI: 10.1002/app.42632

INTRODUCTION

Isotactic polypropylene (iPP) is a well-known semi-crystalline thermoplastic polymer which is widely used for various applications because of its outstanding properties such as low cost, easy processing, good mechanical properties, chemical stability, and nontoxicity.[1–4] iPP is a typical polymorphic material with several crystal modifications including monoclinic α-phase,[5,6] trigonal β-phase,[7–10] and orthorhombic γ-phase.[11,12] Among them, α-phase is the most stable crystalline phase and can be obtained under practical processing conditions, while β-iPP is less stable but has higher toughness compared with α-iPP,[13–15] which can only be obtained in large amount under some specific crystallization conditions, for instance, crystallization in a temperature gradient,[16] in the shear field,[17,18] and with the aid of β-nucleating agent.[19,20]

The iPP usually have varying degree and distributions of stereo-regularity since heterogeneous Ziegler–Natta catalysts contain multiple active sites.[21–23] These stereo-defects places on iPP chains, influences the regular movement of molecular chains and affects on the folding manner and helical conformation. Therefore, the tacticity parameters (including the average isotacticity, and distribution of stereo-defects and stereo-regular sequences) of iPP are important parameters determining for most part of the crystallization behaviors, processability, and mechanical properties. In past decades, the relationship between average isotacticity, crystallization behavior, and final mechanical properties were studied in detail.[24–27] However, when it comes to the uniformity of stereo-defect distribution, because of the proprietary reasons and the complexity of ZN-iPP polymerization, it is not easy to adjust the polymerization conditions and to obtain ZN-iPP with similar average isotacticities

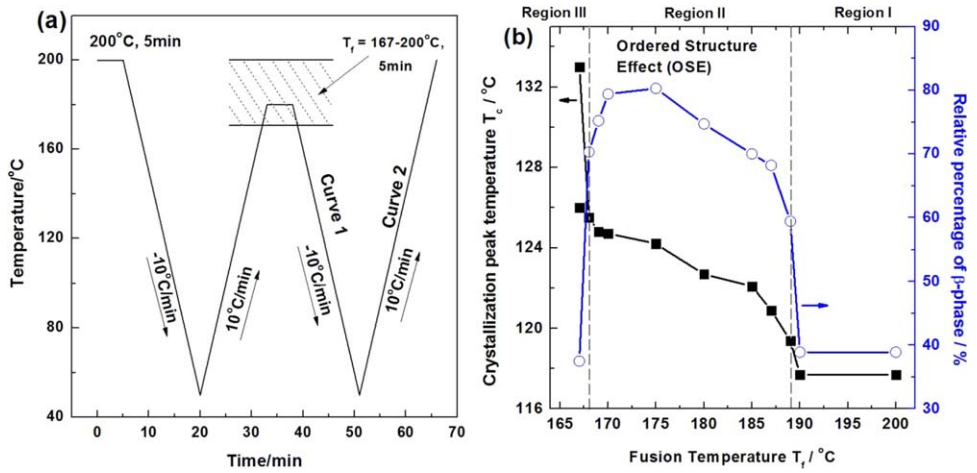

Scheme 1. (a) Schematic illustration of DSC thermal treatment protocol to study the crystallization and melting behavior of iPP with different melt structures[41,42] and (b) Variations of crystallization peak temperature (T_c) and the relative percentage of β-phase (β_c) as a function of fusion temperature (T_f) of iPP nucleated with dual-selective β-nucleating agent (rare earth based β-NA, trade name of WBG-II, concentration of 0.03 wt %).[60,61] [Color figure can be viewed in the online issue, which is available at wileyonlinelibrary.com.]

and molecular masses, but different defect distributions. Therefore, the role of stereo-defect distribution on the crystallization and mechanical properties had rarely been studied, to our best knowledge.

On the other hand, an important issue in polymer crystallization is whether the ordered structures exist in the melt before the occurrence of real crystallization or not.[7,28–32] Recently, more and more evidences were reported, pointing out that some ordered structures may exist in the supercooled polymer melt before the occurrence of real crystallization.[33–39] However, since it is quite difficult to directly measure polymer melt status using the current characterization techniques, a wise method was usually used to explore the effect of ordered structure in polymer crystallization, self-nucleation.[40–43] When heating temperature (fusion temperature, T_f) applied on the polymer is not high enough to make it fully molten, an amount of ordered structures will survive within the melt. Therefore, the content of locally ordered structures can be tuned by controlling the T_f applied on the polymer. Although the physical nature of ordered structures is still under debate, it is commonly accepted that they can serve as self-nucleating agent during the crystallization process, enhance the nucleation density and crystallization rate.[44,45]

More interestingly, many works pointed out that the ordered structures are closely related to β-phase crystallization of iPP. By introducing partially melting iPP fiber to homogeneous supercooled iPP melt, Yan *et al.*[18,46–49] systematically investigated the β-crystallization of iPP/iPP fiber single composite and found that the partly melting of orientated fibers may provide locally ordered structures within certain orientation window, which play very important role in the β-crystallization; Alfonso *et al.*[50–52] studied the formation and relaxation of shear-induced nucleation and found that shear flow and partially molten fiber have similar effect on the formation of β-phase; Shen *et al.*[53,54] explored the combined effect of ordered structures and shear flow on polymorphic nature of β-cylindrites and found that only in the presence of ordered structures can iPP melt form β-cylindrites under the influence of shear flow, showing that ordered structures under shearing is crucial to β-crystallization of iPP. Although the crystallization conditions and components of the above works are quite different from each other, the two-stage characteristics of β-nucleation in these studies are, to some extent, very similar in our opinion: (i) at the early stage of crystallization, the row nucleated α-lamellae forms firstly along the shear stress / fiber direction. (ii) Then, β-nucleation takes places on the edge of row nucleated α-lamellae and a competitive growth of both α- and β-crystal occurs. To our surprise, this two-stage characteristic of β-nucleation in the cases mentioned above is similar with that in the case of dual-selective β-NA,[55–58] revealing the possibility that the β-nucleation under different crystallization conditions may share the same physical nature.

Based on the above understandings, recently we[59] tuned the heating temperature (fusion temperature, T_f) to control the melt structure of iPP [namely, to control content of ordered structures in iPP melt as described in Scheme 1(a)]. In this way, we studied the role of melt structure in the β-crystallization behavior of iPP nucleated with various β-nucleating agents (β-NAs). Surprisingly, for iPP nucleated with the dual-selective β-NA (which can induce both α- and β-crystallization, depending on the applied processing conditions, such as the rare earth-based β-NA with the trade name of WBG-II, and the widely used *N*, *N*′-dicyclohexyl-2, 6-naphthalenedicarboxamide, DCNDCA), the melt structure plays very important role in the β-phase crystallization. When T_f is proper for the melt to preserve an amount of ordered structures, these ordered structures can exhibit high β-nucleation efficiency under the influence of dual-selective β-NA, resulting in the elevated crystallization temperature and significant increase of the relative percentage of the β-phase [(β_c, measured by DSC as shown in Scheme 1(b)], which was called Ordered Structure Effect (OSE). In the following studies,[60,61] we explored the dynamic crystallization behavior and isothermal crystallization kinetics of β-iPP with

different melt structures, to explore the crystallization kinetics characteristics of OSE behavior.

The results above elucidated first evidence that for iPP nucleated with dual-selective β-NA, the presence of ordered structures in iPP melt plays a very important role. Moreover, considering the previous reports concerning the role of ordered structures under shearing or orientation in β-crystallization of iPP[18,53,54] as well as the studies focusing the β-crystallization behavior of iPP induced by dual-selective β-NAs,[55,62,63] our findings provided a very important speculation: under all the crystallization conditions mentioned above, the β-nucleation mechanism might be similar, where ordered structures play a determining role. A possible mechanism depicting a two-step β-nucleation behavior of iPP had been proposed in the previous studies. However, the physical nature of the OSE behavior is still not fully understood, which need further investigations.

Recently, by precisely tuning the polymerization conditions in Ziegler–Natta polymerization process, we prepared a series of iPP samples with similar molecular masses and average isotacticities but different uniformities of stereo-defect distribution.[64,65] The role of stereo-defect distribution in the crystallization behavior,[65–67] polymorphic composition[60,68,69] as well as mechanical properties[70,71] of iPP were studied. The results showed that the uniformity of stereo-defect distribution plays an important role in determining the crystallization rate, β-phase crystallization, and mechanical properties of iPP; particularly, the β-phase proportion was found to be closely related to the uniformity of stereo-defect distribution. The well-defined iPP samples with different uniformities of stereo-defect distribution provide an opportunity to explore its role in the occurrence and physical nature of the OSE behavior, which is of great importance in both academic and practical aspects.

EXPERIMENTAL

Materials

Samples studied in this article were iPP for biaxially oriented polypropylene (BOPP) film, produced in the Spheripol process (Basell) in the two loop reactors, which is one of the most widespread commercial methods to produce PP. The temperature for prepolymerization reactor was controlled at 20°C and 70°C for the main polymerization reactors. The pressure of those three reactors ranged from 3.4 to 4.2 MPa. The cocatalyst was triethylaluminium (TEAL), and the external donor used was cyclohexylmethyldimethoxysilane (CHMDMS). The mole ratio of the cocatalyst/external donor (triethylaluminium/ cyclohexylmethyldimethoxysilane, denoted as Al/Si in this study) was 40, and other conditions remained unchanged. Two different highly activity supported fourth generation Ziegler–Natta ($TiCl_4$=$MgCl_2$) catalysts, ZN-A and ZN-B (the activity of ZN-A was higher than that of ZN-B), were respectively used, and two samples (PP-A and PP-B) were obtained respectively.[65]

The β-NA with trade name WBG-II was supplied by Guangdong Winner Functional Materials (China). WBG-II is heteronuclear dimetal complex of lanthanum and calcium with some specific ligands, which is a kind of irregular block-like crystal whose single crystal diameters is about tens of nanometers. The WBG-II has a general formula of $Ca_xLa_{1-x}(LIG1)_m(LIG2)_n$, where x and $1-x$ is the proportion of Ca^{2+} and La^{3+} ion in the complex, while LIG1 and LIG2 are respectively a dicarboxylic acid and amide-type ligand with coordination numbers of m and n. WBG-II is a typical dual-selective β-NA which enhances both α and β forms in iPP; Moreover, it exhibits self-organization behavior depending on the thermal conditions applied.[56,60,61,72]

Sample Preparation

The iPP pellets and WBG-II were mixed in the mass ratio of 100 : 1 and then extruded by a twin-screw extruder (SHJ-20, Nanjing Giant Machinery, China) and pelletized to obtain master batch. The master batch and iPP were mixed and extruded by twin-screw again to obtain β-iPP. The concentration of WBG-II was 0.03 wt %. To benefit discussion, PP-A and PP-B nucleated with 0.03wt % WBG-II were denoted as WPP-A and WPP-B, respectively.

Differential Scanning Calorimetry (DSC)

All the calorimetric experiments were performed with Mettler Toledo DSC1 (Mettler, Switzerland) differential scanning calorimeter (DSC) under nitrogen atmosphere (50 mL min^{-1}). The temperature scale calibration was performed using indium as a standard to ensure reliability of the results. Five mg round samples were used. All the melting curves were fitted using Peakfit 4.12 software according to literatures.[73,74] The relative percentage of β-crystal (β_c) were estimated by the following expression:

$$\beta_c = X_\beta/(X_\beta + X_\alpha) \quad (1)$$

where the degree of crystallinities X_α and X_β associated with α and β phases, respectively.

In DSC measurement, the thermal treatment described in Scheme 1(a) was applied to create iPP with different melt structures[41]: The sample was firstly heated to 200°C and held for 5 min to erase any previous thermal history. Then it was cooled to 50°C at 10°C min^{-1} to create "standard" thermal history. After that, it was heated to different fusion temperatures (T_f, ranging from 167°C to 200°C) at 10°C min^{-1} and held for 5 min to create different melt structures, namely, to control the presence and content of the ordered structures in the melt. Then, it was cooled down to 50°C at 10°C min^{-1}. Finally, it was heated to 200°C at 10°C min^{-1}.

Wide-Angle X-ray Diffraction

Wide-Angle X-ray Diffraction (WAXD) patterns were recorded with a DX-1000 diffractometer. The wavelength of CuKα was λ=0.154 nm and the spectra were recorded in the 2θ range of 5–35°, a scanning rate of 2° min^{-1}, and a scanning step of 0.02°.

The content of β-crystal was determined according to standard procedures described in the literatures,[75] employing the following equation:

$$k_\beta = \frac{H_\beta(110)}{H_\beta(110)+H_\alpha(110)+H_\alpha(040)+H_\alpha(130)} \quad (2)$$

k_β denotes the relative content of β-crystal form (WAXD), H_α(110), H_α(040), and H_α(130) are the intensities of the strongest peaks of α-form attributed to the (110), (040), and (130) planes

Table I. Molecular Structural Parameters of PP-A and PP-B

				mm[d]			mr[d]			rr[d]		
Sample	XS/%[a]	Isotacticity/%[b]	M_w[c]	mmmm	mmmr	rmmr	mmrr	mmrm+rmrr	rmrm	rrrr	mrrr	mrrm
PP-A	3.8	96.6	365050	95.07	1.59	0.41	2.12	0.57	0.30	0.61	0.45	0.88
PP-B	3.9	96.4	347150	94.78	1.47	0.53	2.17	0.71	0.31	0.65	0.48	0.90

[a] Xylene soluble fraction at room temperature according to ASTM D5492;
[b] Isotacticity were obtained from high temperature ^{13}C NMR at 120°C;
[c] Molecular mass and distribution were performed by GPC at 130°C.
[d] Samples were extracted in *n*-heptane for 24 h at desired temperature and then the insoluble fraction was collected and dried for high resolution ^{13}C NMR measurement, in order to exclude the influence of the atactic fraction.

of monoclinic cell, respectively. H_β (110) is the intensity of the strongest (110) diffraction peak of the trigonal β-form.[8,9]

Polarized Optical Microscopy

The crystalline morphology of the β-nucleated iPP was observed on a Leica DMIP polarized optical microscopy (POM) equipped with a Linkam THMS 600 hot stage under crossed polarizer and a digital camera. The samples were firstly made of thin slices (about 20 μm) on hot stage at 200°C, and the put on the polarizing microscope to observe. The samples were heated to 200°C quickly, stayed 5 min to eliminate the thermal history, and then cooled down to 100°C at 5°C min^{-1}, crystal morphology was recorded with the help of digital camera. It should be noted that since we found that during the crystallization process of the samples, when the T_c temperature decreases to 100°C, the crystallization of the samples is already finished, and the crystalline morphology will not change with the further decrease of T_c. Therefore, we selected 100°C as the end temperature of cooling process.

Scanning Electron Microscopy

The morphology observation (Scanning Electronic Microscopy, SEM) was performed on a JSM-5900 LV environmental scanning electron microscope at an accelerating voltage of 20 kV. Before SEM characterizations, the surfaces of all the samples were coated with a thin layer of gold by ion sputtering. All the samples were etched for 2 h in a solution containing 1.3 wt % potassium permanganate (KM_nO_4), 32.9 wt % concentrated sulfuric acid (H_2SO_4), and 65.8 wt % concentrated phosphoric acid (H_3PO_4), according to the procedure proposed in references.[71,76]

Rheological Measurement

The rheological measurements were performed with a stress-controlled Gemini 200 rheometer (Malvern Instruments, UK) in the linear viscoelastic regime under a nitrogen atmosphere, and the selected stress was 10 Pa. Testing sample disks with a diameter of 25 mm and a thickness of 1.5 mm were prepared by compression molding of the PP pellets at 190°C for 5 min. Each specimen was initially heated to 220°C and held for 5 min. A dynamic temperature sweep mode was applied at an oscillation frequency of 0.1 rad s^{-1}, and the temperature was subsequently decreased at a rate of 3°C min^{-1} until the solidification of iPP occurred.

RESULTS AND DISCUSSION

Microstructure and Crystallization of iPP

The iPP used in this study (PP-A and PP-B) are polymerized by two different highly activity supported fourth generation Ziegler–Natta catalysts. Their microstructure and crystallization behavior are studied using ^{13}C NMR, DSC thermal fractionation technic (successive self-nucleation and annealing, SSA), FT-IR, and DSC in the previous works.[65,66,68,77,78] A brief summary of their microstructure information is given here as shown in Table I.

As can be seen from Table I, the average isotacticities (XS and isotacticity) of PP-A and PP-B are nearly same. However, the concentrations of the "mmmm" and "mmmr" pentads of PP-B are lower than that of PP-B, meanwhile, the contents of other pentads of PP-B representing less regular and irregular structures are higher than that of PP-A, indicating that the stereo-defect distribution of PP-B is more uniform than that of PP-A.

The DSC cooling and subsequent heating curves of pure iPP (PP-A and PP-B) and β-nucleated iPP (WPP-A and WPP-B) are recorded as shown in Figure 1.

Figure 1 reveals that for pure iPP, the crystallization temperature of PP-A is obviously higher than that of PP-B; for β-nucleated iPP, the crystallization temperature of WPP-A is higher than that of WPP-B.

On the melting curves, after the addition of 0.03 wt % WBG-II, multiple peaks emerge on the melting curve of WPP-B, suggesting the formation of an amount of β-phase; meanwhile, no β-melting peaks can be observed on the melting curve of WPP-A, revealing that PP-A is less favorable for β-phase crystallization compared with PP-B, which is in accordance with the previous studies.[60,68]

The differences in crystallization and melting behavior between PP-A and PP-B, WPP-A and WPP-B above are attributed to the different uniformities of stereo-defect distribution of the samples. A deep analysis was given in the previous studies,[60,68] claiming that PP-A with less uniform stereo-defect distribution has higher degree of regular movement of the molecular chains because of the less restrain from the stereo-defects; further, the crystallization rate and the α-nucleation ability of PP-A is obviously higher than that of PP-B, resulting in higher crystallization temperature and lower tendency for β-phase crystallization.

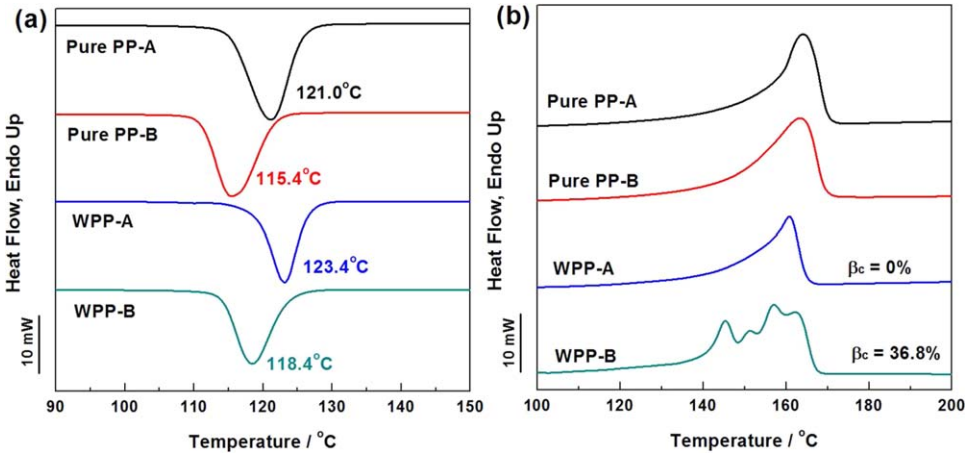

Figure 1. (a) Cooling curves and (b) subsequent heating curves of the pure iPP and β-nucleated iPP. [Color figure can be viewed in the online issue, which is available at wileyonlinelibrary.com.]

Crystallization and Melting Behavior of iPP with Different Melt Structures

The melt structure (i.e., content of ordered structures in the melt) of the sample is controlled by tuning the fusion temperature (T_f) according to Scheme 1(a). In this way, the impact of melt structure on the crystallization and melting behavior of WPP-A and WPP-B is studied.

Crystallization Behavior. The crystallization curves of WPP-A and WPP-B with different melt structures [Curve 1 in Scheme 1(a)] are shown in Figure 2. The variations of crystallization peak temperature (T_c) of the samples are plotted as a function of T_f in Figure 3.

Figures 2 and 3 reveal that when $T_f > 189$°C, the crystallization peak temperatures T_c of both WPP-A and WPP-B stay constant, suggesting the constant nucleation density of the melt; as T_f steps into the range of 168–189°C, T_c increases gradually with the decrease of T_f because of the increase of the amount of ordered structures within the melt. Meanwhile, it can be seen that the increment of T_c of WPP-A (whose distribution of stereo-defect is less uniform) is obviously smaller than that of WPP-B; when T_f becomes lower than 168°C, the crystallization peaks of WPP-A and WPP-B significantly widen and a second crystallization peak located at high temperature range emerges on the cooling curves, indicating that T_f is so low that the large ordered entities can survive in the melt, which are large enough to induce annealing or recrystallization in the course of subsequent cooling and therefore induce in a second crystallization peak in high temperature range.[41,42,45]

On the other hand, although the uniformities of stereo-defect distribution of WPP-A and WPP-B are different, the upper and lower limiting temperatures of Region II (defined in the previous study,[59] indicated by the dotted lines in Figure 3) of the samples are identical, suggesting that the uniformity of stereo-defect distribution has little influence on the temperature range of Region II.

Melting Behavior. The melting curves of WPP-A and WPP-B with different melt structures are shown in Figure 4. The

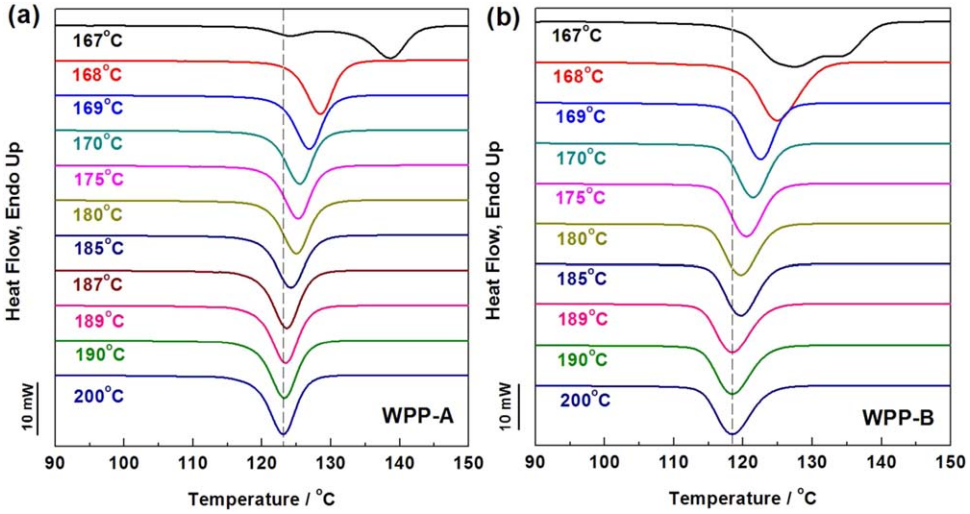

Figure 2. (a) Cooling curves and (b) subsequent heating curves of WPP-A and WPP-B cooled after held at the indicated fusion temperatures for 5 min. [Color figure can be viewed in the online issue, which is available at wileyonlinelibrary.com.]

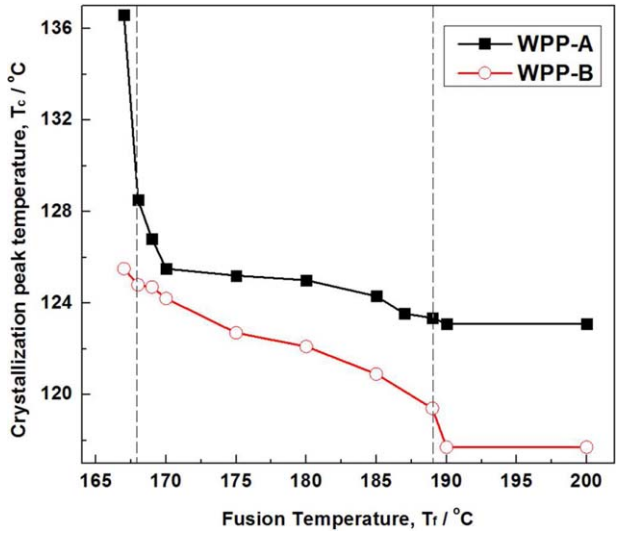

Figure 3. Variation of crystallization peak temperature T_c as a function of fusion temperature T_f. [Color figure can be viewed in the online issue, which is available at wileyonlinelibrary.com.]

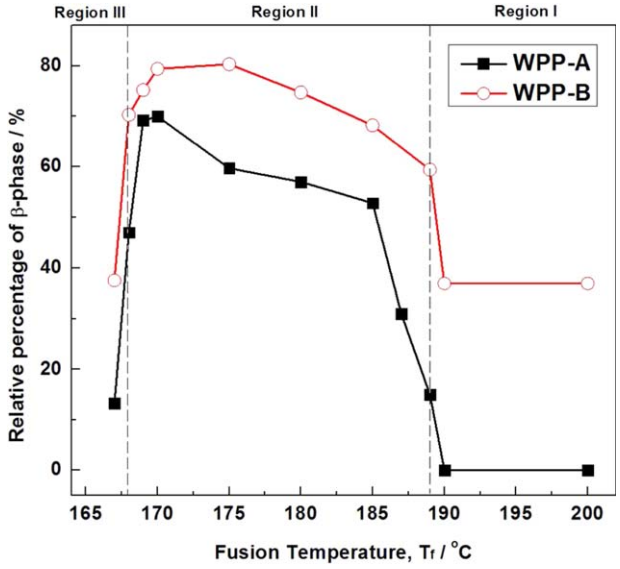

Figure 5. Plots of the relative contents of β-phase β_c of WPP-A and WPP-B as a function of the fusion temperature T_f. [Color figure can be viewed in the online issue, which is available at wileyonlinelibrary.com.]

relative percentage of β-phase β_c is calculated and plotted as a function of the fusion temperature T_f as shown in Figure 5.

As can be seen from Figures 4 and 5, for WPP-A, the β-phase can hardly form when $T_f > 189$°C because of the strong α-nucleation tendency of the sample;[60,68,69] Once T_f steps into 168–189°C, the β-melting peak appears on the heating curve, and β_c increases gradually from 0% ($T_f > 189$°C) to 69.8% at maximum (T_f=170°C), indicating the occurrence of Ordered Structure Effect (OSE); when T_f decreases to lower than 168°C, β_c decreases sharply because of the presence of large α-phase entities as described above. According to the variation of T_c and β_c of WPP-A, the T_f ranges of higher than 189°C, 168–189°C and lower than 168°C are defined as Regions I, -II, and -III, respectively. For WPP-B, similar variation trend of T_c and β_c as T_f decreases is observed, and its upper and lower limiting temperatures of Region II are identical to that of WPP-A.

The WAXD is performed on the samples after held at the indicated T_f of 170°C and 200°C for 5 min respectively and then cooled to room temperature, as shown in Figure 6. The β-phase content k_β is calculated as shown in Figure 6.

Figure 6 reveal that for both WPP-A and WPP-B, the β-phase content k_β increases evidently once T_f decreases from 200°C to 170°C, which is in accord with DSC analysis above.

The results above also reveal that OSE behavior can provide unsurpassed β-nucleation efficiency for iPP and encourage the formation of high proportion of β-phase; for WPP-A with less uniform stereo-defect distribution and stronger α-nucleation

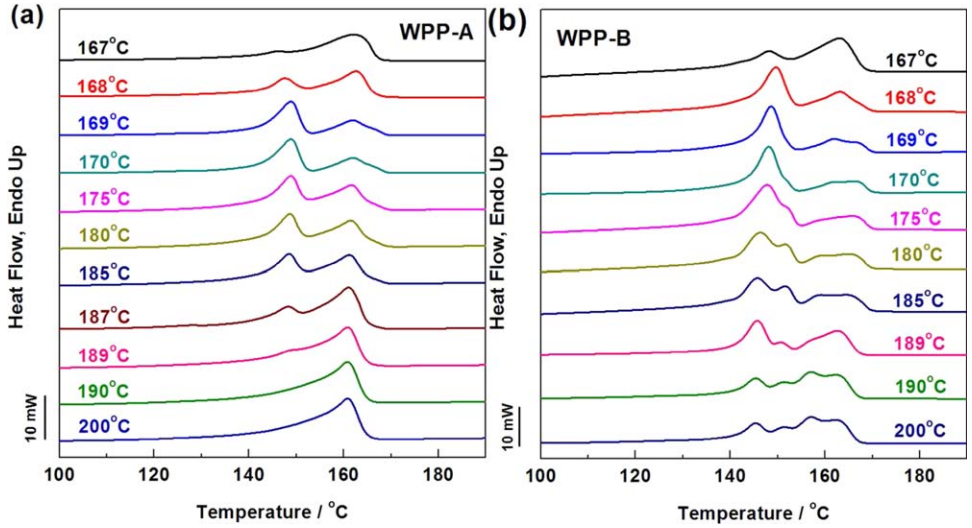

Figure 4. Heating curves [Curve 2 in Scheme 1(a)] of (a) WPP-A and (b) WPP-B after held at the indicated T_f and then cooled to 50°C. The cooling and heating rates are 10°C min^{-1}. [Color figure can be viewed in the online issue, which is available at wileyonlinelibrary.com.]

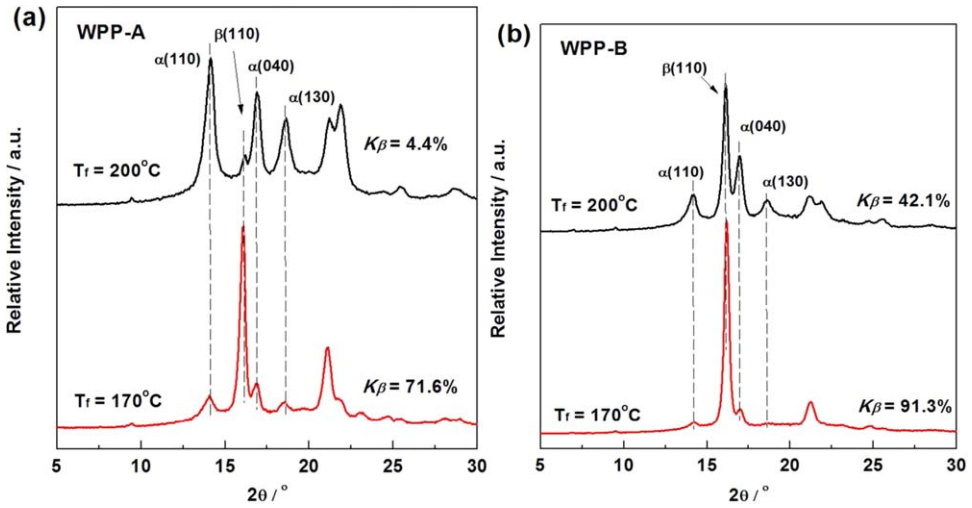

Figure 6. WAXD profiles of (a) WPP-A and (b) WPP-B. [Color figure can be viewed in the online issue, which is available at wileyonlinelibrary.com.]

ability, the occurrence of OSE behavior can also enhance its the β-phase crystallization; meanwhile, it is observed that the OSE behavior can lead to a higher amount of β-phase in WPP-B, which has more uniform stereo-defect distribution and is more favorable for β-crystallization.

On-Line Measurement During Crystallization Process

Rheological Measurement. In this section, the rheological approach is used to investigate the structural evolution during the early stage of crystallization of the samples with different melt structures. From a viewpoint of rheology, polymer crystallization can be simplified as liquid-to-solid transition or biphasic system, where the rigid crystals suspend in amorphous melt.[61,70,79] The dynamic storage modulus and viscosity will proportionally increase with elevated solid-like degree (crystallinity). Therefore, the evolving spectrum of storage modulus upon cooling can be used to describe the early stage of crystallization. The storage modulus as a function of temperature for WPP-A and WPP-B is recorded during the cooling process as shown in Figure 7.

It can be observed that for both WPP-A and WPP-B, the inflection point of the curve gradually shift towards higher temperature as T_f varies from 200°C to 185°C, 178°C, and 170°C, revealing that the crystallization occurs at higher temperature because of the increase of the amount of ordered structures; on the other hand, at the same T_f, the inflection point of WPP-A is higher than that of WPP-B, indicating that when the OSE takes place, WPP-A with less uniform stereo-defect distribution crystallizes at higher temperature compared with WPP-B, which is in accordance with the DSC analysis above.

POM Observation. The online POM is performed to directly observe the morphology evolution of the sample. The obtained POM images of WPP-A and WPP-B during cooling process after held at different T_fs (170°C and 200°C, respectively) are shown in Figure 8.

Because of the limiting resolution, the α and β phases can hardly be differentiated from the POM images. However, one can clearly see the differenence in morphology evolution of the samples during the crystallization process. When T_f=200°C, the number of nuclei during the early stage of crystallization of WPP-A is obviously higher than that of WPP-B, resulting in much smaller crystallite sizes after the completion of crystallization; when T_f=170°C, the nucleation density of both WPP-A and WPP-B increase evidently and finally results in smaller sized crystallites of the samples. The crystalline sizes of WPP-A are quite close to that of WPP-B, showing strong nucleation effect of the OSE behavior.

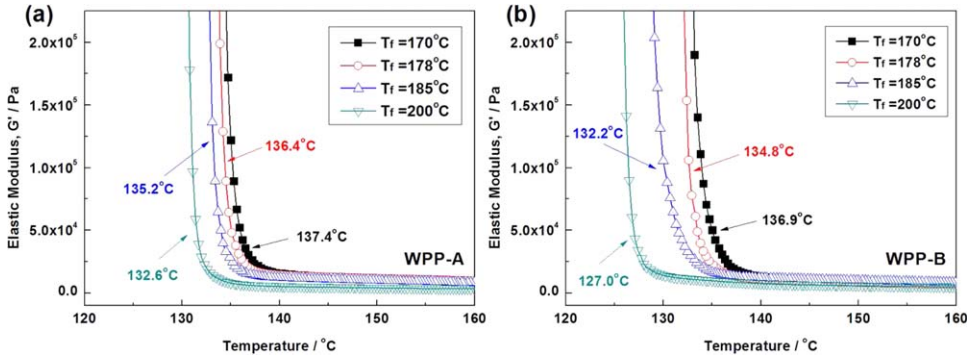

Figure 7. Storage modulus as a function of temperature of WPP-A and WPP-B cooled from the indicated fusion temperature T_f at the rate of 3°C min^{-1}. [Color figure can be viewed in the online issue, which is available at wileyonlinelibrary.com.]

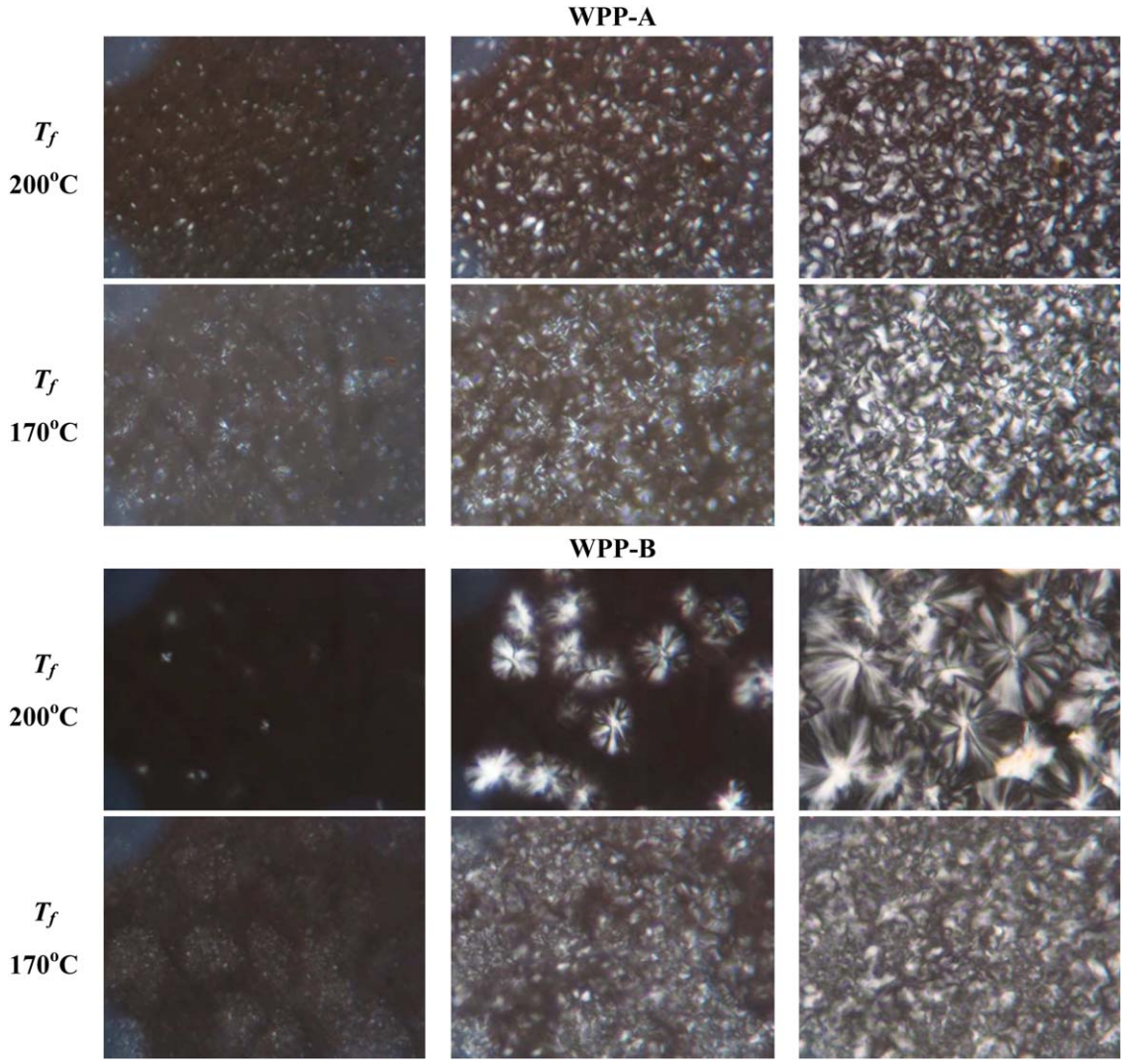

Figure 8. POM images of WPP-A and WPP-B cooled from after held at the indicated fusion temperature T_f (170°C and 200°C, respectively). The cooling rate applied is 5°C min^{-1}. [Color figure can be viewed in the online issue, which is available at wileyonlinelibrary.com.]

SEM Observation. The SEM morphological result of the hot-molded samples after etching is shown in Figure 9.

When T_f =200°C, no β-crystals (bright spherulites in the SEM image) can be observed in WPP-A, while only some large β-spherulites with diameter about 20 μm can be observed in WPP-B; As T_f comes to 170°C, for both WPP-A and WPP-B, the spherulite sizes decrease and the β-phase content increases obviously. However, the crystalline morphology of WPP-A is somewhat different from that of WPP-B: the β-spherulites of WPP-B are fully developed compared with that of WPP-A, which almost fill up the screen; meanwhile, the β-spherullites of WPP-A is less developed, and many dark α-spherulites distribute on the screen. The different morphologies of WPP-A and WPP-B above might be attributed to their different molecular structures and different crystallization behaviors.

Discussions

From the results above, the physical nature of the T_f temperature range of Region II is speculated in this section. Since the OSE behavior is based on the molecular thermodynamics and classical self-nucleation theory, the temperature ranges of self-nucleation domains and the equilibrium melting temperatures of PP-A and PP-B are calculated.

The Lower Limiting Temeprature of Region II. The self-nucleation and annealing behaviors of PP-A and PP-B are studied according to the standard procedures proprosed by the elegant literatures:[41–45] (i) Sample is firstly held at 200°C for 5 min to erase any thermal history and then cooled to 50°C at 10°C min^{-1} to create the "standard" thermal history. (ii) After that, it is heated to the selected fusion temperature T_f and held for 5 min. Then it is cooled to 50°C and subsequently heated to 200°C, where the heating and cooling rates are 10°C min^{-1}. The cooling and heating curves of PP-A and PP-B are recorded as shown in Figure 10.

Figures 10 and 11 suggest that the lower limiting temperatures of the exclusive self-nucleation domain (Domain II in the self-nucleation theory) of both PP-A and PP-B are 168°C, which is

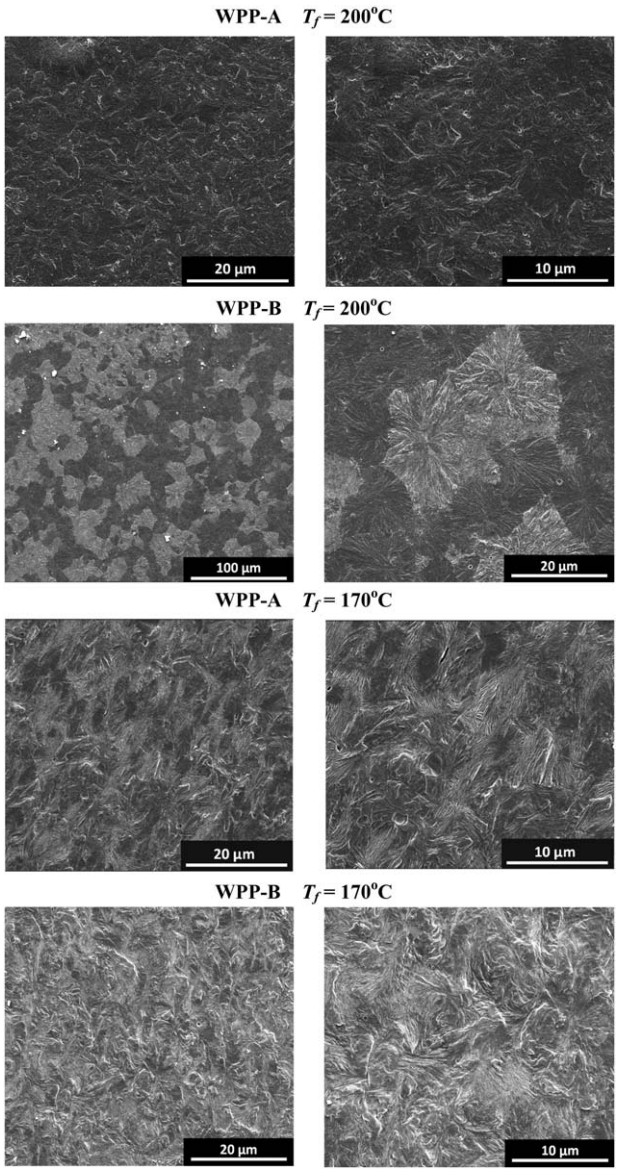

Figure 9. SEM images (after etching) of the iPP nucleated with 0.03 wt % WBG-II after held at the indicated fusion temperature (T_f) for 5 min and then cooling to room temperature.

identical with the lower limiting temperature of Region II in the OSE behavior as studied above. Usually, it is accepted that this temperature corresponds to the melting temperature of all the ordered entities that can induce annealing or recrystallization during the subsequent cooling.

The Upper Limiting Temperature of Region II. With respect to the upper limiting temperature of Region II, it is surprise to find it being far above the apparent melting temperature of the sample, which is quite different from the upper limiting temperature of Domain II (172°C as shown in Figure 10) in classical self-nucleation theory. To explain this, the equilibrium melting temperatures (T_m^0) of PP-A and PP-B are measured by extrapolating the plot of melting temperature (T_m) versus crystallization temperature (T_{cISO}) to $T_{cISO}=T_m=T_m^0$ in terms of the Hoffman-Weeks Equation:[80]

$$T_m=(1-1/\gamma)T_m^0+T_{cISO}/\gamma \quad (3)$$

where γ is the ratio of the crystal thickness to the thickness of the initial nucleus at crystallization temperature T_{cISO}. The obtained melting curves and the extrapolation of PP-A and PP-B are shown in Figure 12.

Figure 12 shows that the T_m^0 of PP-A and PP-B are 185.9°C and 185.3°C respectively, which are quite close to their upper limiting temperatures of Region II (189°C). Therefore, a possible explanation is that, the upper limiting temperature of Region II in OSE behavior corresponds to the fusion temperature in which a complete melting can be obtained. However, differing from the classical self-nucleation theory, the thermal stability of the ordered structures in β-iPP melt is so strong that they can only be totally destroyed when the fusion temperature reaches the equilibrium melting temperature; in this process, the presence of dual-selective β-NA must be of great importance.

In general, for both PP-A and PP-B whose uniformities of stereo-defect distribution are different, the OSE behavior can be induced at wide fusion temperature range of Region II.

CONCLUSIONS

In this study, two β-nucleated isotactic polypropylene (WPP-A and WPP-B) with nearly similar molecular mass and average isotacticity, but different uniformities of stereo-defect distribution (the stereo-defect distribution of PP-B is more uniform than that of PP-A) were prepared, their crystallization behavior and polymorphic composition with the variation of melt structure were studied by DSC, WAXD, POM, and SEM to explore the role of stereo-defect distribution in the Ordered Structrure Effect of iPP. The conclusions can be drawn as follows:

1. Preliminary characterization revealed that β-phase can hardly form in WPP-A because of its strong tendency of α-nucleation caused by its less uniform stereo-defect distribution, while WPP-B is more favorable for the formation of β-crystals.
2. As fusion temperature (T_f) decreases, similar variation trends of crystallization temperature and β-phase proportion β_c can be observed from WPP-A and WPP-B, indicating that OSE behavior takes place in both samples, providing unsurpassed β-nucleation efficiency and therefore induce β-crystallization even in WPP-A which is less favorable for β-crystallization; moreover, the upper and limiting temperatures of Region II of WPP-A and WPP-B are identical, suggesting that the uniformity of stereo-defect distribution determines the value of β_c but has little influence on the upper and lower limiting temperatures of Region II.
3. Through investigating the self-nucleation behavior of PP-A and PP-B, it was found that the lower limiting temperatures of the exclusive self-nucleation domain of both PP-A and PP-B are identical with the lower limiting temperatures of Region II in OSE behavior (168°C), revealing that the lower limiting temperatures of SN and OSE may have the same physical

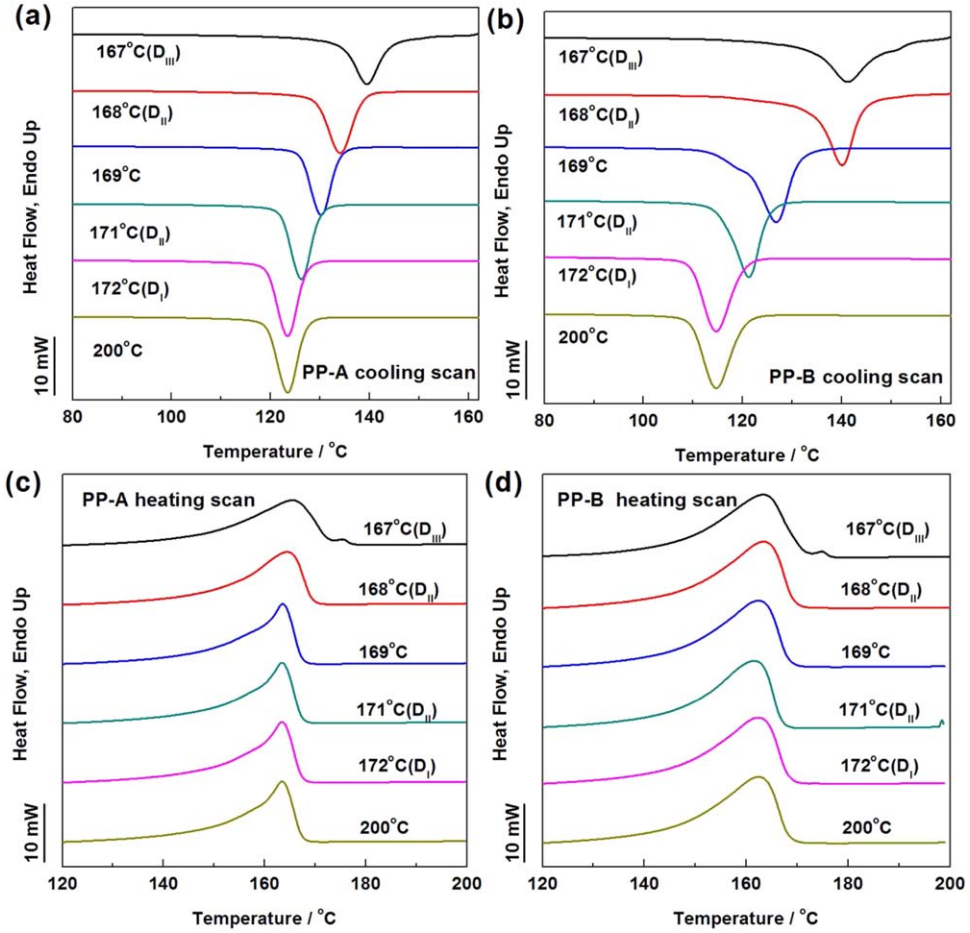

Figure 10. Cooling curves of (a) PP-A and (b) PP-B after held at the indicated T_f for 5 min; Subsequent heating curves of (c) PP-A and (d) PP-B. The cooling and heating rates are 10°C min^{-1}. (D_I, D_{II}, and D_{III} means Domain I, Domain II, Domain III, respectively). [Color figure can be viewed in the online issue, which is available at wileyonlinelibrary.com.]

nature, which corresponds to the melting temperature of all the ordered entities that can induce annealing or recrystallization during the subsequent cooling.

4. The calculation of equilibrium melting temperature (T_m^0) showed that T_m^0 of both PP-A and PP-B are quite close to their upper limiting temperatures of Region II in OSE

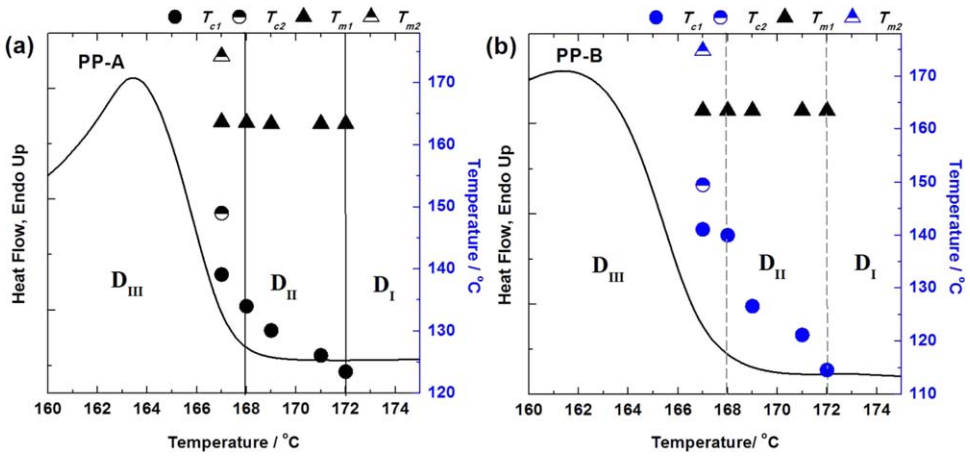

Figure 11. DSC heating curves of PP-A and PP-B (10°C min^{-1}). Superimposed on the DSC curves is a representation of the self-nucleation Domains (vertical lines) and data. On the right hand side *Y*-axis, the crystallization peak temperature (T_c) and melting point (T_m) are presented as a function of the fusion temperature (T_f). (D_I, D_{II}, and D_{III} means Domain I, Domain II, Domain III, respectively). [Color figure can be viewed in the online issue, which is available at wileyonlinelibrary.com.]

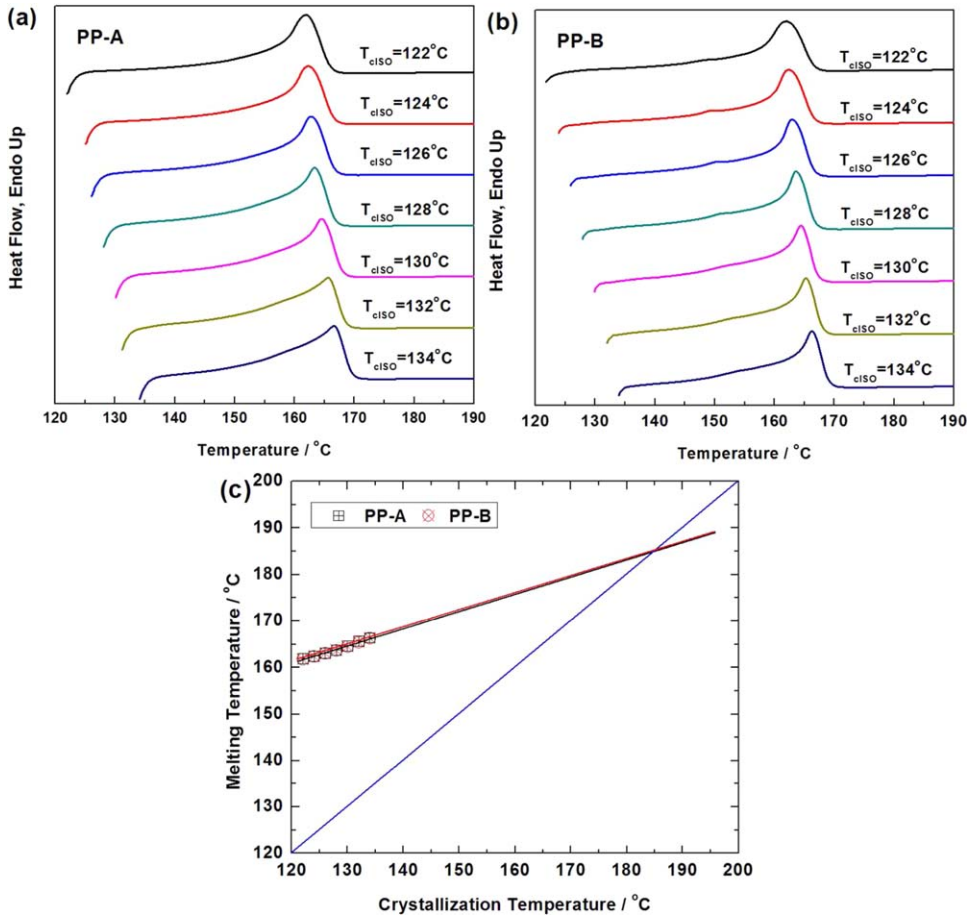

Figure 12. DSC melting curves of (a) PP-A and (b) PP-B obtained at the heating rate of 10°C min^{-1} after isothermally crystallization for 60 min; (c) Plots of observed melting temperature (T_m) of iPP as a function of crystallization temperature (T_{clSO}). [Color figure can be viewed in the online issue, which is available at wileyonlinelibrary.com.]

behavior (189°C), which helps to understand the physical nature of OSE behavior.

ACKNOWLEDGMENTS

We express our sincerely thanks to the Sichuan University Scientific Research Foundation for Young Teachers (2012SCU11075), Zhejiang Provincial Natural Science Foundation of China (Grant No. LQ14E030001) and National Science Foundation of China (NSFC 51203106, NSFC 21404063) for the financial support. The authors are also grateful for K.C. Wong Magna Fund of Ningbo University.

REFERENCES

1. Karger-Kocsis, J.; Wanjale, S. D.; Abraham, T.; Bárány, T.; Apostolov, A. A. *J. Appl. Polym. Sci.* **2010**, *115*, 684.
2. Abraham, T. N.; Wanjale, S. D.; Barany, T.; Karger-Kocsis, J. *Compos. A Appl. Sci. Manuf.* **2009**, *40*, 662.
3. Horvath, Z.; Menyhárd, A.; Doshev, P.; Gahleitner, M.; Varga, J.; Tranninger, C.; Pukánszky, B. *J. Therm. Anal. Calorim.* to appear. **2014**, *118*, 235.
4. Kmetty, A.; Barany, T.; Karger-Kocsis, J. *Prog. Polym. Sci.* **2010**, *35*, 1288.
5. Natta, G.; Corradini, P. *Nuovo Cim.* **1960**, *15*, 40.
6. Kang, J.; Li, J.; Chen, S.; Zhu, S.; Li, H.; Cao, Y.; Yang, F.; Xiang, M. *J. Appl. Polym. Sci.* **2013**, *130*, 25.
7. Lotz, B. *Eur Phys J E* **2000**, *3*, 185.
8. Dorset, D. L.; McCourt, M. P.; Kopp, S.; Schumacher, M.; Okihara, T.; Lotz, B. *Polymer* **1998**, *39*, 6331.
9. Ferro, D. R.; Meille, S. V.; Bruckner, S. *Macromolecules* **1998**, *31*, 6926.
10. Varga, J. *J. Macromol. Sci. B* **2002**, *41*, 1121.
11. Bruckner, S.; Phillips, P. J.; Mezghani, K.; Meille, S. V. *Macromol. Rapid Commun.* **1997**, *18*, 1.
12. De Rosa, C.; Auriemma, F.; DiCapua, A.; Resconi, L.; Guidotti, S.; Camurati, I.; Nifant'ev, IE.; Laishevtsev, IP. *J. Am. Chem. Soc.* **2004**, *126*, 17040.
13. Grein, C. *Adv. Polym. Sci.* **2005**, *188*, 43.
14. Wang, C.; Dai, W.; Zhang, Z.; Mai, K. *J. Therm. Anal. Calorim.* **2013**, *111*, 1585.
15. Lin, Z.; Chen, C.; Guan, Z.; Li, M.; Guo, G.; Xian, J.; Li, W. *J. Therm. Anal. Calorim.* **2013**, *114*, 229.

16. Pawlak, A.; Piorkowska, E. *Colloid Polym. Sci.* **2001**, *279*, 939.
17. Varga, J.; Karger-Kocsis, J. *J. Polym. Sci. B-Polym. Phys.* **1996**, *34*, 657.
18. Liu, Q.; Sun, X.; Li, H.; Yan, S. *Polymer* **2013**, *54*, 4404.
19. Mathieu, C.; Thierry, A.; Wittmann, J. C.; Lotz, B. *J. Polym. Sci. B Polym. Phys.* **2002**, *40*, 2504.
20. Lu, Q.; Dou, Q. *J. Polym. Res.* **2009**, *16*, 555.
21. Busico, V.; Cipullo, R. *Prog. Polym. Sci.* **2001**, *26*, 443.
22. Chum, P. S.; Swogger, K. W. *Prog. Polym. Sci.* **2008**, *33*, 797.
23. Kissin, Y. V.; Fruitwala, H. A. *J. Appl. Polym. Sci.* **2007**, *106*, 3872.
24. De Rosa, C.; Auriemma, F.; Ballesteros, O.; Resconi, L.; Camurati, I. *Chem. Mater.* **2007**, *19*, 5122.
25. De Rosa, C.; Auriemma, F. *J. Am. Chem. Soc.* **2006**, *128*, 11024.
26. De Rosa, C.; Auriemma, F.; Paolillo, M.; Resconi, L.; Camurati, I. *Macromolecules* **2005**, *38*, 9143.
27. De Rosa, C.; Auriemma, F.; De Lucia, G.; Resconi, L. *Polymer* **2005**, *46*, 9461.
28. Strobl, G. *Eur. Phys. J. E* **2000**, *3*, 165.
29. Lauritzen, J. J. I.; Hoffman, J. D. *J. Appl. Phys.* **1973**, *44*, 4340.
30. Muthukumar, M. *Eur. Phys. J. E* **2000**, *3*, 199.
31. Strobl, G. *Prog. Polym. Sci.* **2006**, *31*, 398.
32. Li, L.; de Jeu, W. Flow-induced mesophases in crystallizable polymers. Interphases and Mesophases in Polymer Crystallization II. Advances in Polymer Science; Springer: Berlin Heidelberg, German, **2005**; p 75.
33. Gee, R. H.; Lacevic, N.; Fried, L. E. *Nat. Mater.* **2006**, *5*, 39.
34. Sanz, A.; Nogales, A.; Puente-Orench, I.; Jimenez-Ruiz, M.; Ezquerra, T. A. *Phys. Rev. Lett.* **2011**, *107*, 025502.
35. Matsuba, G.; Kanaya, T.; Saito, M.; Kaji, K.; Nishida, K. *Phys. Rev. E* **2000**, *62*, 1.
36. Nitash, P.; Balsara, C. L. *Phys. Rev. Lett.* **1996**, *77*, 3847.
37. Kaji, K.; Nishida, K.; Kanaya, T.; Matsuba, G.; Konishi, T.; Imai, M. Spinodal crystallization of polymers: Crystallization from the unstable melt. In Interphases and Mesophases in Polymer Crystallization III. Advances in Polymer Science; Allegra, G., Ed.; Springer: Berlin Heidelberg, German, **2005**; p 187.
38. Cong, Y.; Hong, Z.; Zhou, W.; Chen, W.; Su, F.; Li, H.; Li, X.; Yang, K.; Yu, X.; Qi, Z.; Li, L. *Macromolecules* **2012**, *45*, 8674.
39. Cong, Y.; Hong, Z.; Qi, Z.; Zhou, W.; Li, H.; Liu, H.; Chen, W.; Wang, X.; Li, L. *Macromolecules* **2010**, *43*, 9859.
40. Li, X.; Su, F.; Ji, Y.; Tian, N.; Lu, J.; Wang, Z.; Li, L. *Soft Mater.* **2013**, *9*, 8579.
41. Fillon, B.; Wittmann, J.; Lotz, B.; Thierry, A. *J. Polym. Sci. B Polym. Phys.* **1993**, *31*, 1383.
42. Muller, A. J.; Arnal, M. L. *Prog. Polym. Sci.* **2005**, *30*, 559.
43. Cavallo, D.; Gardella, L.; Portale, G.; Muller, A. J.; Alfonso, G. C. *Polymer* **2014**, *55*, 137.
44. Lorenzo, A. T.; Müller, A. J. *J. Polym. Sci. B-Polym. Phys.* **2008**, *46*, 1478.
45. Lorenzo, A. T.; Arnal, M. L.; Sánchez, J. J.; Muller, A. J. *J. Polym. Sci. B Polym. Phys.* **2006**, *44*, 1738.
46. Li, H.; Yan, S. *Macromolecules* **2011**, *44*, 417.
47. Li, H.; Sun, X.; Yan, S.; Schultz, J. M. *Macromolecules* **2008**, *41*, 5062.
48. Cheng, S.; Hu, W.; Ma, Y.; Yan, S. *Polymer* **2007**, *48*, 4264.
49. Li, H.; Jiang, S.; Wang, J.; Wang, D.; Yan, S. *Macromolecules* **2003**, *36*, 2802.
50. Cavallo, D.; Portale, G.; Balzano, L.; Azzurri, F.; Bras, W.; Peters, G. W.; Alfonso, G. C. *Macromolecules* **2010**, *43*, 10208.
51. Cavallo, D.; Azzurri, F.; Balzano, L.; Funari, S. S.; Alfonso, G. C. *Macromolecules* **2010**, *43*, 9394.
52. Azzurri, F.; Alfonso, G. C. *Macromolecules* **2005**, *38*, 1723.
53. Zhang, B.; Chen, J.; Ji, F.; Zhang, X.; Zheng, G.; Shen, C. *Polymer* **2012**, *53*, 1791.
54. Zhang, B.; Chen, J.; Cui, J.; Zhang, H.; Ji, F.; Zheng, G.; Heck, B.; Reiter, G.; Shen, C. *Macromolecules* **2012**, *45*, 8933.
55. Varga, J.; Menyhard, A. *Macromolecules* **2007**, *40*, 2422.
56. Luo, F.; Geng, C.; Wang, K.; Deng, H.; Chen, F.; Fu, Q.; Na, B. *Macromolecules* **2009**, *42*, 9325.
57. Dong, M.; Guo, Z. X.; Yu, J.; Su, Z. Q. *J. Polym. Sci. B-Polym. Phys.* **2009**, *47*, 314.
58. Dong, M.; Guo, Z.; Yu, J.; Su, Z. *J. Polym. Sci. B Polym. Phys.* **2008**, *46*, 1725.
59. Kang, J.; Weng, G.; Chen, Z.; Chen, J.; Cao, Y.; Yang, F.; Xiang, M. RSC Adv. **2014**, *4*, 29514.
60. Kang, J.; Chen, Z.; Zhou, T.; Yang, F.; Chen, J.; Cao, Y.; Xiang, M. *J. Polym. Res.* **2014**, *21*, 1.
61. Kang, J.; Zhang, J.; Chen, Z.; Yang, F.; Chen, J.; Cao, Y.; Xiang, M. *J. Polym. Res.* **2014**, *20*, 1.
62. Luo, F.; Wang, K.; Ning, N.; Geng, C.; Deng, H.; Chen, F.; Fu, Q.; Qian, Y.; Zheng, D. *Polym. Adv. Technol.* **2011**, *22*, 2044.
63. Dong, M.; Jia, M.; Guo, Z.; Yu, J. *Chin. J. Polym. Sci.* **2011**, *29*, 308.
64. Kang, J.; Yang, F.; Wu, T.; Li, H.; Cao, Y.; Xiang, M. *Eur. Polym. J.* **2012**, *48*, 425.
65. Kang, J.; Yang, F.; Wu, T.; Li, H.; Liu, D.; Cao, Y;. Xiang, M. *J. Appl. Polym. Sci.* **2012**, *125*, 3076.
66. Kang, J.; Li, J.; Chen, S.; Peng, H.; Wang, B.; Cao, Y.; Li, H.; Chen, J.; Gai, J.; Yang, F.; Xiang, M. *J. Appl. Polym. Sci.* **2013**, *129*, 2663.
67. Kang, J.; Cao, Y.; Li, H.; Li, J.; Chen, S.; Yang, F.; Xiang, M. *J. Polym. Res.* **2012**, *19*, 1.
68. Kang, J.; Gai, J.; Li, J.; Chen, S.; Peng, H.; Wang, B.; Cao, Y.; Li, H.; Chen, J.; Yang, F.; Xiang, M. *J. Polym. Res.* **2013**, *20*, 1.

69. Chen, Z.; Wang, B.; Kang, J.; Peng, H.; Chen, J.; Yang, F.; Cao, Y.; Li, H.; Xiang, M. *Polym. Adv. Technol.* **2014**, *25*, 353.

70. Kang, J.; Xiong, B.; Liu, D.; Cao, Y.; Chen, J.; Yang, F.; Xiang, M. *J. Polym. Res.* **2014**, *21*, 1.

71. Peng, H.; Wang, B.; Gai, J.; Chen, J.; Yang, F.; Cao, Y.; Li, H.; Kang, J.; Xiang, M. *J. Appl. Polym. Sci.* **2014**, *131*, 40027.

72. Kang, J.; Peng, H.; Wang, B.; Chen, Z.; Li, J.; Chen, J.; Cao, Y.; Li, H.; Yang, F.; Xiang, M. *J. Appl. Polym. Sci.* **2014**, *131*, 40115.

73. Yamamoto, Y.; Inoue, Y.; Onai, T.; Doshu, C.; Takahashi, H.; Uehara, H. *Macromolecules* **2007**, *40*, 2745.

74. Kang, J.; Chen, J.; Cao, Y.; Li, H. *Polymer* **2010**, *51*, 249.

75. Turner-Jones, A.; Aizlewood, J.; Beckett, D. *Makromol. Chem.* **1964**, *75*, 134.

76. Olley, R. H.; Bassett, D. C.; Blundell, D. *J. Polymer* **1986**, *27*, 344.

77. Kang, J.; Wang, B.; Peng, H.; Li, J.; Chen, J.; Gai, J.; Cao, Y.; Li, H.; Yang, F.; Xiang, M. *Polym. Adv. Technol.* **2014**, *25*, 97.

78. Kang, J.; Wang, B.; Peng, H.; Chen, J.; Cao, Y.; Li, H.; Yang, F.; Xiang, M. *Polym. Bull.* **2014**, *71*, 563.

79. Wang, K.; Zhou, C.; Tang, C.; Zhang, Q.; Du, R.; Fu, Q.; Li, L. *Polymer* **2009**, *50*, 696.

80. Celli, A.; Fichera, A.; Marega, C.; Marigo, A.; Paganetto, G.; Zannetti, R. *Eur. Polym. J.* **1993**, *29*, 1037.